

Article

Hierarchically Porous Carbon Cloth–Polyaniline (CC–PANI) Composite Supercapacitor Electrodes with Enhanced Stability

Svetlana V. Stakhanova ^{1,2}, Ilya S. Krechetov ¹, Kristina E. Shafigullina ^{1,*}, Tatiana L. Lepkova ¹,
Valentine V. Berestov ¹, Eugene S. Statnik ¹, Zlatotsveta E. Zyryanova ², Elena A. Novikova ¹
and Alexander M. Korsunsky ^{3,*}

¹ Department of Physical Chemistry, University of Science and Technology MISIS, Moscow 119049, Russia

² Department of Analytical Chemistry, Mendeleev University of Chemical Technology, Moscow 125047, Russia

³ Trinity College, University of Oxford, Broad St., Oxford OX1 3BH, UK

* Correspondence: k.shafigullina@misis.ru (K.E.S.); alexander.korsunsky@trinity.ox.ac.uk (A.M.K.)

Abstract: In this work, hierarchically porous composites were prepared in the form of activated carbon cloth (CC) Busofit T–1–055 filled with an electrically conductive polymer, polyaniline (PANI), for use as pseudocapacitive electrodes of electrochemical supercapacitors (SCs). CC fibers have high nanoporosity and specific surface area, so it was possible to deposit (via the chemical oxidative polymerization of aniline) a significant amount of PANI on them in the form of a thin layer mainly located on the inner surface of the pores. Such morphology of the composite made allowed the combining of the high capacitive characteristics of PANI with the reversibility of electrochemical processes, high columbic efficiency and cyclic stability rather typical for carbon materials of double-layer SCs. The highest capacitance of composite electrodes of about 4.54 F/cm² with high cyclic stability (no more than 8% of capacity loss after 2000 charge–discharge cycles with a current density of 10 A/cm²) and columbic efficiency (up to 98%) was achieved in 3 M H₂SO₄ electrolyte solution when PANI was synthesized from an aniline hydrochloride solution with a concentration of 0.25 M. Trasatti analysis revealed that 27% of specific capacitance corresponded to pseudocapacitance, and 73% to the double-layer capacitance.

Keywords: electrically conductive polymer; polyaniline; carbon cloth; supercapacitor; chemical polymerization; pseudocapacitance; double-layer capacitance



Citation: Stakhanova, S.V.; Krechetov, I.S.; Shafigullina, K.E.; Lepkova, T.L.; Berestov, V.V.; Statnik, E.S.; Zyryanova, Z.E.; Novikova, E.A.; Korsunsky, A.M. Hierarchically Porous Carbon Cloth–Polyaniline (CC–PANI) Composite Supercapacitor Electrodes with Enhanced Stability.

Crystals **2024**, *14*, 457. <https://doi.org/10.3390/cryst14050457>

Academic Editor: John A. Mydosh

Received: 7 April 2024

Revised: 2 May 2024

Accepted: 10 May 2024

Published: 12 May 2024



Copyright: © 2024 by the authors. Licensee MDPI, Basel, Switzerland. This article is an open access article distributed under the terms and conditions of the Creative Commons Attribution (CC BY) license (<https://creativecommons.org/licenses/by/4.0/>).

1. Introduction

Supercapacitors (SCs) are electrochemical energy storage devices that operate by storing charge at the surfaces of electrodes. By the mechanism of charge accumulation, they can be subdivided into electrical double-layer SCs (EDLCs), pseudocapacitors, and hybrid SCs [1–3].

In EDLCs, charge storage occurs in an electrical double layer at the electrode–electrolyte interface mainly via physical adsorption of ions on the electrode surface. Electrode materials for EDLCs are usually made from activated carbon which has a high specific surface area due to its porous structure as well as other carbon materials such as carbon nanotubes, graphene and carbon onion structures [4–8]. In addition to high specific power, an important feature of EDLCs is high cyclic stability—they can withstand up to 1 million charge–discharge cycles without significant change of characteristics. These features make EDLCs irreplaceable in those cases when high power and impulse character of energy release is required, for example, at start-up of car engines, diesel locomotives, turbines, regeneration of transport braking energy, etc. [9–11]. Moreover, EDLCs are increasingly used as storage devices in distributed energy generation systems and in autonomous hybrid power supply systems as well as in backup energy storage systems [12,13].

Nevertheless, the specific energy capacity of EDLCs is significantly lower than for a lithium-ion battery which limits their independent application to some extent. Using

pseudocapacitive electrode materials allows the increasing of the energy capacitance of SCs up to several times. The mechanism of charge accumulation by pseudocapacitive materials is based on fast reversible redox reactions on the surface of the active material accompanied by a change in the valence state and charge transfer through the surface of the electrode–electrolyte interface. Additionally, pseudocapacitance can be caused by the intercalation of charge carriers into the tunnels or pores of the electrode [9,14–16]. Unlike the processes occurring in lithium-ion batteries, this intercalation does not cause phase changes in the electrode material. When a pseudo-capacitor operates, this involves transfer of charge across the electrolyte/electrode interface as in the batteries. However, the voltage response of the pseudocapacitive electrode to the accumulated charge exhibits capacitor-type character. In this case, the electrode potential during the faradaic reaction changes with the charge linearly, or approximately linearly, resulting in a measurable capacitance. Since the origin of capacitance does not arise from traditional charge separation, as in the case of classical capacitors or EDLCs, the term “pseudocapacitance” was used. It was proposed to use transition metal compounds such as RuO₂ and MnO₂, other metal oxides, or metal sulfides, nitrides and carbides as pseudocapacitive materials [17–20]. Some electrically conductive polymers such as polyaniline (PANI), polypyrrole, polythiophene and their derivatives exhibit rapid and reversible redox processes in certain electrolytes, and thus have attracted considerable interest as pseudocapacitive materials for energy storage applications due to their low cost and light weight [21–25]. Apparently, PANI has the greatest prospects for commercialization since aniline is a common and relatively low-cost monomer due to the manufacturability of the polymerization process [21,26–28]. There are strong arguments that the nature of the PANI capacitance is due not only to the rapid reversible redox reaction, but also to the formation of a double layer on interface at the polymer fibrils/internal solution. This makes PANI-based pseudocapacitive materials even more interesting for further study [29].

It should be noted that in order to further increase the window of operating potential, energy and power density, a new type of electrochemical energy storage device has been developed, which is known as a hybrid capacitor. Generally, hybrid capacitors utilize both the double layer capacitance and faradaic reaction to charge storage. These are (a) quite promising devices that can use composite electrodes based on materials with double-layer capacitance in combination with materials with pseudocapacitance; (b) asymmetric devices with one EDL electrode and another pseudocapacitive or battery-type electrode; and (c) asymmetric SCs with one pseudocapacitive electrode and another rechargeable battery-type electrode.

Composite electrodes can integrate carbon-based materials with pseudocapacitive materials (e.g., metal oxides and electrically conductive polymers) and thus combine both electrostatic and faradaic charge storage mechanisms in a single electrode. The carbon-based materials not only provide EDL capacitance but also provide a high-surface-area framework or matrix that allows a uniform deposition of pseudocapacitive materials and a 3D charge distribution [30].

A critical drawback limiting the use of pseudocapacitive materials in SC electrodes is their low cyclic stability which manifests in a decrease of capacitive performance by more than two times after hundreds of cycles. In the case of conducting polymers, such as PANI, this phenomenon can be caused by several factors. First of all, this is the contribution of irreversible oxidation and reduction processes that occur upon charging SCs above a certain threshold potential, leading to the transition of PANI into non-conductive forms—pernigraniline and leucoemeraldine. Second is the mechanical destruction of PANI fibers upon the intercalation of counterions with solvent molecules during the charging process [15,21,25,27].

To increase cyclic stability, it was proposed to deposit PANI on solid carriers such as carbon nanotubes, graphene, etc. [29–35] Another approach is doping using acids with bulk anions, such as mellitic acid, to ensure free changes in the PANI macromolecule conformation during the counterion transportation process [15,24,35–37]. Such approaches

allow the obtaining of materials with the required combination of characteristics, but the high cost of components constrains their commercialization.

Carbon cloths are inexpensive and highly conductive materials with excellent mechanical flexibility and strength; they hold great promise as an electrode material for flexible SCs [38–40]. Additionally, they also have been used as an inert substrate material for the growth of various metal oxides like TiO_2 and MnO_2 for various applications [41–45].

In the present work, it was proposed to use an activated CC to create PANI-containing composites with high capacity and cyclic stability. Analysis of the data in the literature indicates that carbon cloths can be successfully used as a substrate for the PANI nanostructure formation; however, the majority of researchers use carbon fibers with small specific surface areas [46–51]. Fibers of activated CCs have high porosity and a specific surface area, the modification of which by electrically conductive polymer can lead to significant growth of the capacitive performance. Additionally, the use of electrode materials based on CC is promising in flexible electronics systems [52–54]. These considerations were taken into account in choosing the method of chemical oxidative polymerization of aniline in the presence of CC for the formation of PANI as a composite filler. On the one hand, it is known that PANI obtained by chemical polymerization demonstrates a tendency to form thin layers on the surface of substrates in the polymerizing solution [55]. On the other hand, it should be taken into account that the chemical method of aniline polymerization can be scaled up quite easily unlike the electrochemical method and opens excellent prospects for implementation in production.

The aim of the present work was to obtain CC–PANI composites based on activated carbon cloth owing to its high porosity and specific surface area, for SCs' high performance electrode materials and to study the contribution of PANI pseudocapacitance toward the total electrical capacitance of the obtained composite materials.

2. Materials and Methods

2.1. Carbon Cloth

Carbon cloth (CC) "Busofit" T-1-055 produced by OJSC «SvetlogorskKhimvolokno» (Svetlogorsk, Republic of Belarus) was used as the textile carrier structure for obtaining the composite materials. According to the manufacturer's specifications, this CC is characterized by high adsorption capacity values for methylene blue (about 400 mg/g) and iodine (about 130%); additionally, a limiting volume of sorption space for benzene vapor is at least 0.55 cm³/g. Surface density was 110 ± 20 g/m². Rectangular swatches of an area of 80 × 120 mm² were used to obtain the composite samples.

2.2. Modification of Carbon Cloth with Polyaniline

The mass of aniline required to obtain a solution with a given concentration was dissolved in a 1 M HCl solution. The CC sample was soaked in 50 mL of the resulting solution for 40 min. Polymerization was carried out for 40 min at room temperature by gradually adding 50 mL of $(\text{NH}_4)_2\text{S}_2\text{O}_8$ (oxidizing agent) in the form of solution of equivalent concentration. After this, the modified cloth was washed in a 1 M HCl solution, and then the material was dried in air until the mass became constant. The resulting composites were labeled BP-0, BP-0.125, BP-0.250 and BP-0.300, where BP means «Busofit–PANI composite» and the number is the molar concentration of aniline in the solution used for modification (respectively, 0, 0.125, 0.250 and 0.300 mol/L).

2.3. FTIR Spectrophotometry

FTIR-spectrophotometer Nicolet iS20 (Thermo Fisher Scientific Inc., Waltham, MA, USA) was used to obtain FTIR-spectra of CC and CC–PANI composites in KBr pellets.

2.4. Scanning Electron and Dual-Beam Microscopy

Microphotographs of the samples were obtained using TESCAN VEGA COMPACT scanning electron microscope (SEM) and TESCAN AMBER dual-beam scanning electron microscope (TESCAN Holding Group, Brno, Czech Republic).

Unmodified and modified samples were cut out and fixed on a standard aluminum pin stub using conductive silver paint. Before transferring the samples into the vacuum chamber of the electron-ion microscope TESCAN AMBER, a thin (~50 nm) layer of gold nanoparticles was sputtered onto the sample surface using Quorum Q150R ES Magnetron sputtering machine (Quorum Technologies Ltd., Laughton, United Kingdom). This FIB-SEM system combines a gallium liquid metal ion source for sample milling and a field emission gun scanning electron microscope (FEG-SEM) for high-resolution imaging.

For tomographic serial sectioning, the gallium ion current was set to 1 nA at 30 keV. The sectioning plane spacing was set to 50 nm over an area of $10 \times 7 \mu\text{m}^2$ resulting in 100 slice images and a total dwell time of 1 h.

High-resolution imaging (2048×2048 pixels) was performed using the in-lens secondary electron detector. The electron current was set to 300 pA at 5 keV. Image acquisition took 100 s per frame.

2.5. Fabrication of a Supercapacitor Cell

To prepare the electrodes, CC-PANI composite samples were cut into circles of 25 mm diameter. Using these electrodes, symmetric two-electrode supercapacitor cells were fabricated. The electrodes were impregnated with 1 M or 3 M aqueous solutions of H_2SO_4 as electrolyte, separated by a 25 μm thick membrane material 3501-1240M-A (Celgard, LLC, Charlotte, NC, USA), and placed between two titanium cylindrical current collectors held together with a clamp.

2.6. Cyclic Voltammetry and Galvanostatic Charge-Discharge

The electrochemical characteristics of CC and CC-PANI composites were studied by cyclic voltammetry and galvanostatic charge-discharge methods. The measurements were carried out using potentiostat/galvanostat Elins P30S (Elins, LLC, Moscow, Russia) and a HIT ASK 2.5.10.8 Analyzer (YAROSTANMASH, LLC, Moscow, Russia).

Capacitance of the supercapacitor cells C/F , specific capacitance of the material per 1 cm^2 of electrode C^* (F/cm^2), cell resistance R (Ohm), energy efficiency η_E (%) and charge efficiency η_Q (%) of the supercapacitors were calculated from the galvanostatic charge-discharge (GCD) test results according to Equations (1)–(5)

$$C = I \times \Delta t_{\text{dis}} / \Delta U, \quad (1)$$

$$R = \Delta U' / 2I, \quad (2)$$

$$C^* = 2C / S, \quad (3)$$

$$\eta_Q = (\Delta t_{\text{dis}} / \Delta t_{\text{ch}}) \times 100\%, \quad (4)$$

$$\eta_E = (W_{\text{dis}} / W_{\text{ch}}) \times 100\%, \quad (5)$$

where I is the discharge current (A); Δt_{dis} is the discharge time (s); ΔU is the cell voltage change during discharge after subtraction the ohmic voltage drop (V); S is the electrode area (mm^2); $\Delta U'$ is the ohmic voltage drop on the cell at the beginning of the discharge, (V); Δt_{ch} is the charge time (s); W_{dis} is the energy received during SC discharge (J); W_{ch} is energy spent on the SC charge (J).

The energies W_{dis} and W_{ch} were calculated by numerical integration of the areas under the discharge and charge curves, respectively, of the current-by-voltage product as a function of time obtained during galvanostatic charge-discharge (GCD) test.

The current–voltage dependences obtained during cyclic voltammetry (CV) were recalculated into the capacitance–voltage dependencies given per unit area of the electrode with Equation (6)

$$C = 2I/(\nu \times S), \quad (6)$$

where I is the current flowing through the cell (A) and ν is the sweep rate (V/s).

2.7. Trasatti Method

The contributions of the «inner» capacitance C_i (associated with the pseudocapacitance) and «outer» capacitance C_o (associated with the capacitance of the electrical double layer—EDL) to the total capacitance C_T (ultimate value at the potential sweep rate tending to zero) of electrode materials were estimated by the Trasatti method, according to the algorithm described in [56], while the total electrical capacitance was determined from the CV curves with Equation (7)

$$C = A/(2 \times \nu \times \Delta U), \quad (7)$$

where A is area of the CV curve, ν is the sweep rate (V/s) and ΔU is the voltage range at CV (V).

The obtained capacitance values were recalculated into area-normalized specific capacitance according to Equation (6).

3. Results and Discussion

FTIR spectra between 2000 and 400 cm^{-1} of the BP-0.250 composite, PANI in salt form, and pure CC BP-0 are given in Figures S1–S3. Compared with the FTIR spectrum of pure CC Busofit T-1-055, the FTIR spectra of CC–PANI composites exhibit several new peaks that are ascribed to the typical absorption mode of PANI. The peaks around 1570 and 1482 cm^{-1} correspond to quinone and benzene ring-stretching deformation, respectively. The absorption band at 1305 cm^{-1} corresponds to π -electron delocalization induced in PANI by protonation. The band characteristic of the conducting protonated form is observed at 1225 cm^{-1} and interpreted as a C-N⁺ stretching vibration in the polaron structure. The intense band at 1140 cm^{-1} is assigned to a vibration mode of the NH⁺ = structure, which is formed during protonation [57,58]. Thus, the spectrum of CC–PANI composites confirms the formation of polyaniline in the form of protonated emeraldine.

The activated CC Busofit T-1-055 used to produce composites consists of intertwined carbon fibers with a diameter of about 5 microns (Figure 1). The specific surface area of CC determined by the BET method is 1271 m^2/g (the specific surface area was determined by the BET method, while pore volume and radius were obtained using the BJH method applied for nitrogen adsorption carried out using a NOVAtouch 2LX Analyzer (Quantachrome Instruments, Boynton Beach, FL, USA)). Adsorption/desorption isotherms and pore size distribution plots for BP-0 and BP-0.250 obtained are presented in Figure S4a,b. Submicron-sized pores are visible on the surface of the CC fibers (Figure 2a). As a result of the chemical polymerization of aniline, layers of PANI with a thickness of about 100–200 nm was formed on the surface of carbon fibers, while an open porous structure was kept (Figure 2b), providing access for the electrolyte to the inner surface of the pores. This morphology of the composites allows the expectation of an effective combination of the double-layer mechanism of energy storage and pseudocapacitance during the SC functioning.

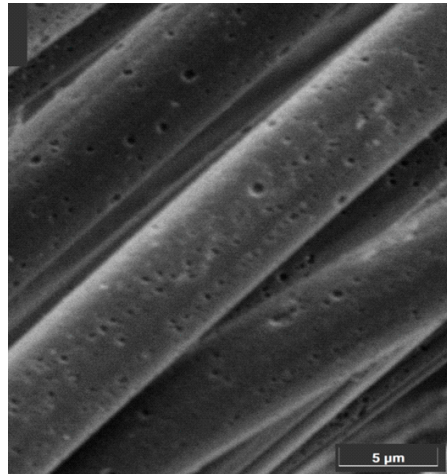


Figure 1. Image of unmodified CC fibers obtained by scanning electron microscopy.

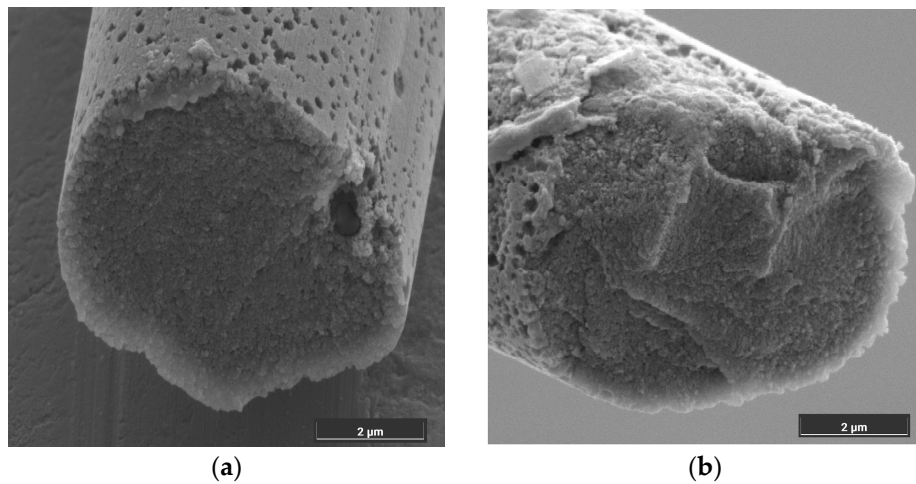


Figure 2. Images of (a) BP-0; (b) BP-0.250 samples obtained by dual-beam scanning electron microscopy.

Figure 3 shows the BP-0 (pure CC) and BP-0.250 (composite) sample images obtained by dual-beam scanning electron microscopy. Figure 3a,b demonstrate a slice of unmodified fiber obtained by ion etching. Figure 3c,d illustrate the end face of the PANI-modified carbon fiber before and after ion microtomy, respectively. As is shown in Figure 3c, the end face shows a large number of formations in the pores, which are apparently formed by PANI particles on the pore walls surface and in the pore volume near the outer surface of the fiber. After removal of a part of the fiber by ion beam, the slice shows pores moving deep into the fiber in the form of channels with a diameter of 10 to 500 nm, and also pore walls going away from the lateral surfaces of the fiber into the depth. At the same time, no PANI particles are visible on the pore walls, which implies that mainly the outer surface of the fiber at the pore exit points is modified. Moreover, Figure 3a–d show that high porosity is retained within both unmodified and PANI-modified CC fibers, which allows energy storage to be realized by a double-layer mechanism.

Figure 4 demonstrates the dependence of the gravimetrically determined mass fraction of PANI in CC–PANI composites on the concentration of aniline in hydrochloric acid solution during polymerization. It can be seen that the mass fraction of PANI does not change at aniline concentrations above 0.250 M. Most probably, during the impregnation of CC with the aniline solution before polymerization, the pores of the CC are saturated with aniline at this concentration, and during polymerization, only the part of the aniline that was in the pores and on the surface near the pores was transformed to anchor on the

fibers' PANI particles. Other PANI particles that were not anchored on the surface and in the pores were removed after washing the composite. It should be noted that the mass fraction of PANI in the composite is controlled by the concentrations of the reagents but does not change when polymerization time is prolonged beyond 40 min.

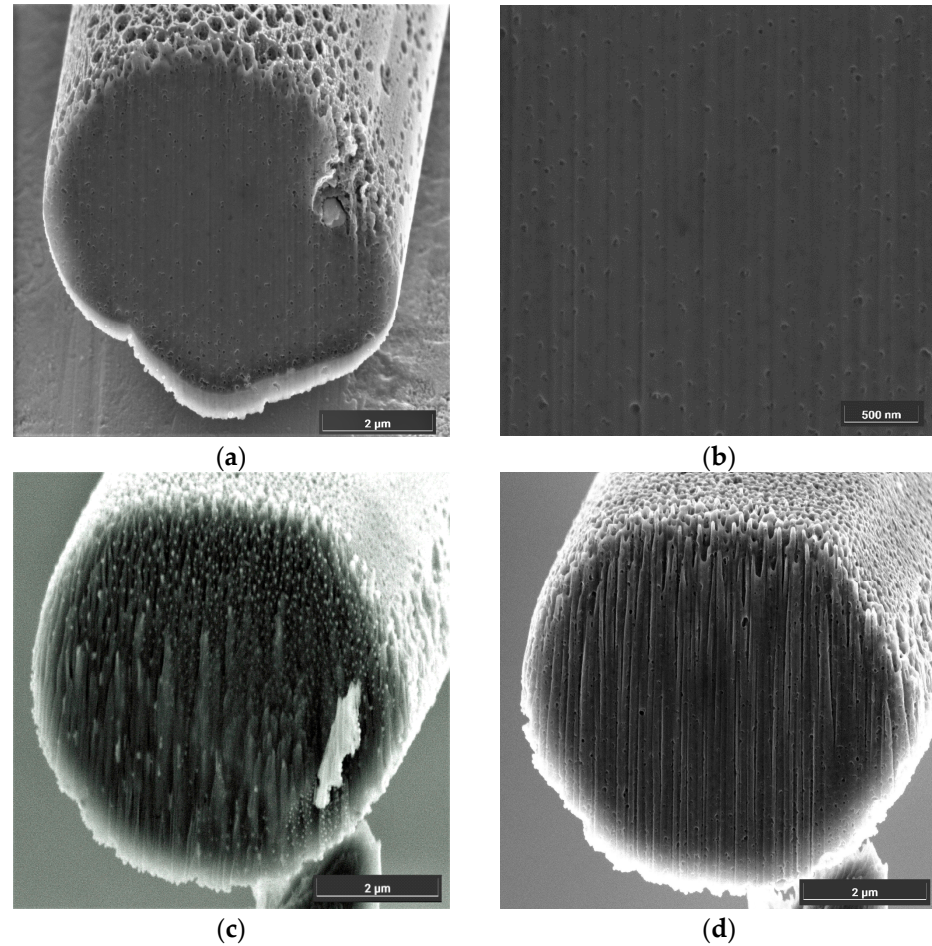


Figure 3. Images of (a,b) BP-0; (c,d) BP-0.250 samples obtained by dual-beam scanning electron microscopy.

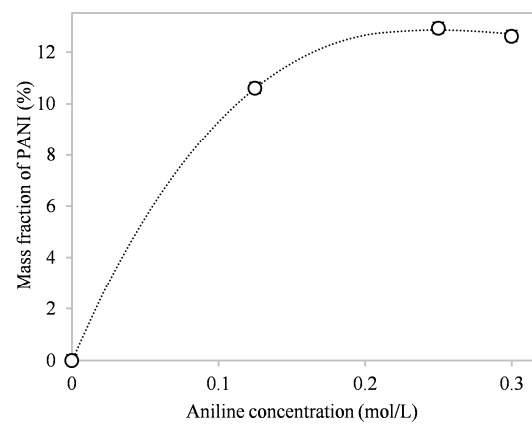


Figure 4. Dependence of the mass fraction of PANI in the composite on the concentration of aniline in hydrochloric acid solution.

Figure 5 illustrates the CV results for SC cells with electrodes made from the prepared composites when using 1 M (Figure 5a) and 3 M (Figure 5b) sulphuric acid solutions as electrolyte at a sweep rate of 10 mV/s.

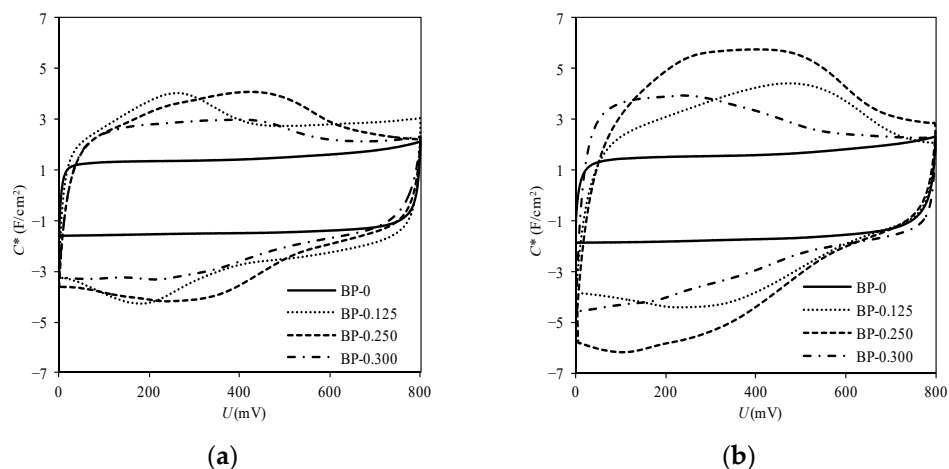
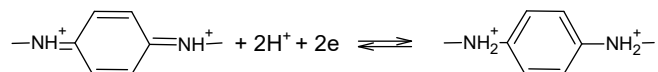


Figure 5. CV of SCs with CC–PANI composite-based electrodes and electrolytes based on (a) 1 M H_2SO_4 and (b) 3 M H_2SO_4 solutions at 10 mV/s.

All composites are characterized by a larger area under the CV curves compared to the unmodified BP–0 cloth, i.e., by higher specific capacitance. At the same time, the CV curves for the composites show peaks indicating the occurrence of reduction and oxidation processes during the charging and discharging of cells, which confirms the presence of pseudocapacitance. The composites BP–0.125 and BP–0.250 demonstrated the highest capacitance.

The reversible redox transition between quinoid and benzoid PANI fragments proceeds via protonation and is accompanied by the diffusion of both protons and counterions:



The position of the redox peak can shift depending on changes in the activity of H^+ ions or in the conditions of the diffusion stage. BP–0.125 sample exhibits a nearly ideal, reversible current peak, suggesting a promising composite morphology of this material in terms of the PANI accessibility to H^+ and HSO_4^- ions. The amount of PANI within the pores of the BP–0.250 composite increases, resulting in slower diffusion, as evidenced by a broadening of the current peak and a shift in its maximum towards higher potentials. Finally, the PANI in the BP–0.300 composite appears to block the pores of the carbon substrate, making it more difficult for electrolyte ions to access these pores, leading to a decrease in the composite capacitance (Figure 5).

Results of the GCD of the SCs at a current density of 10 mA/cm² are presented in Figure 6.

The obtained dependences show that with increasing concentration of aniline in hydrochloric acid solution at polymerization, the specific capacitance of the obtained composites, as well as the values of η_Q and η_E , increase up to aniline concentration equal to 0.250 M, after which they decrease. In contrast, the resistance of SC cells decreases to a minimum at 0.250 M, after which it starts to increase. This is probably associated with the formation of larger PANI particles at higher concentrations of aniline in the polymerization solution, which leads to a partial blocking of the CC pores and a decrease in the electrolyte-accessible pore surface of the electrode material.

In order to investigate the cyclic stability of the electrode materials' capacitive characteristics during long-term cycling, electrodes based on composite BP–0.250, which have the highest specific capacitance, and on unmodified CC BP–0 were subjected to long-term

testing by the GCD method at a current density of 10 mA/cm^2 for 2000 charge–discharge cycles in electrolyte based on 3 M sulphuric acid solution. The results are presented in Figure 7.

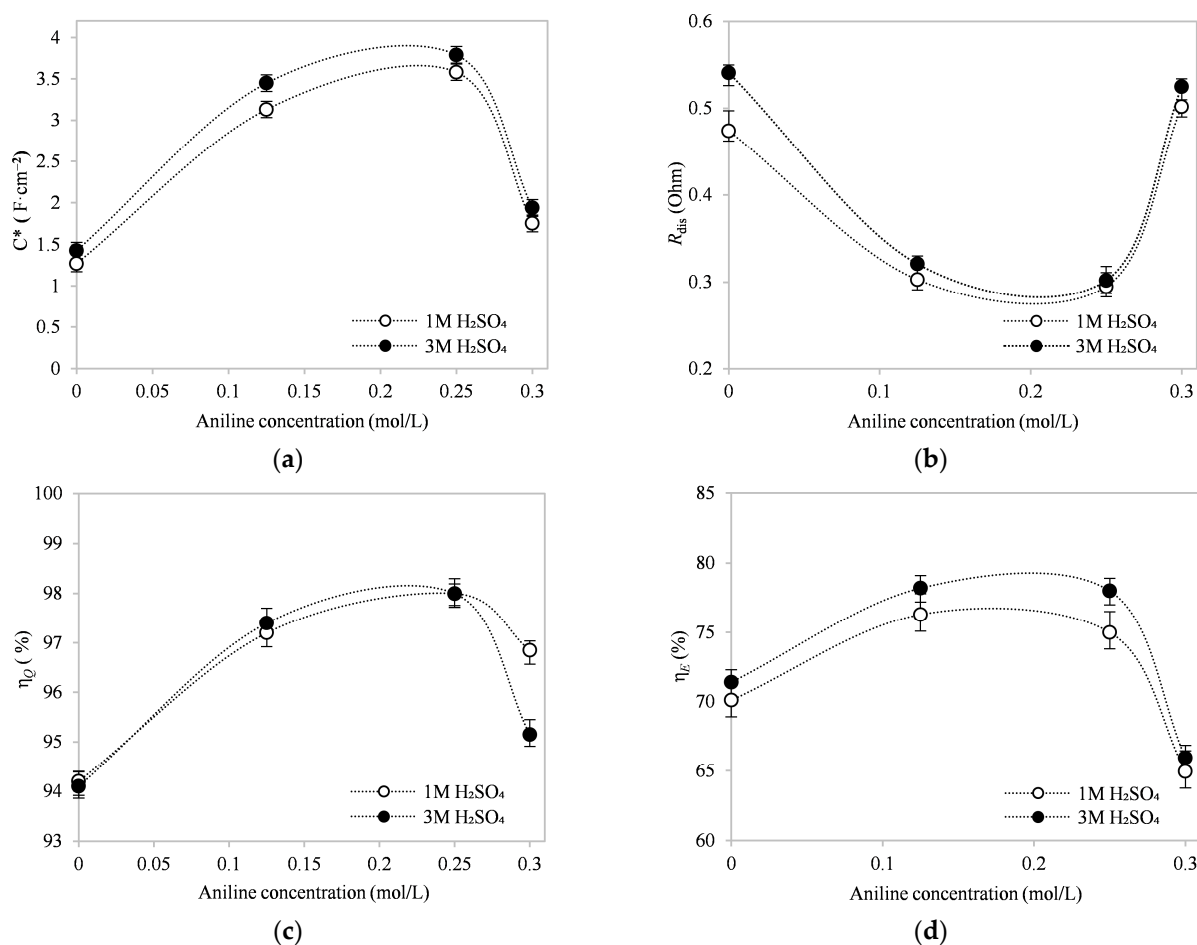


Figure 6. (a) Specific electrical capacitance C^* ; (b) resistance; (c) charge efficiency η_Q ; and (d) energy efficiency η_E determined from GCD as function of aniline concentration during polymerization for CC–PANI composites.

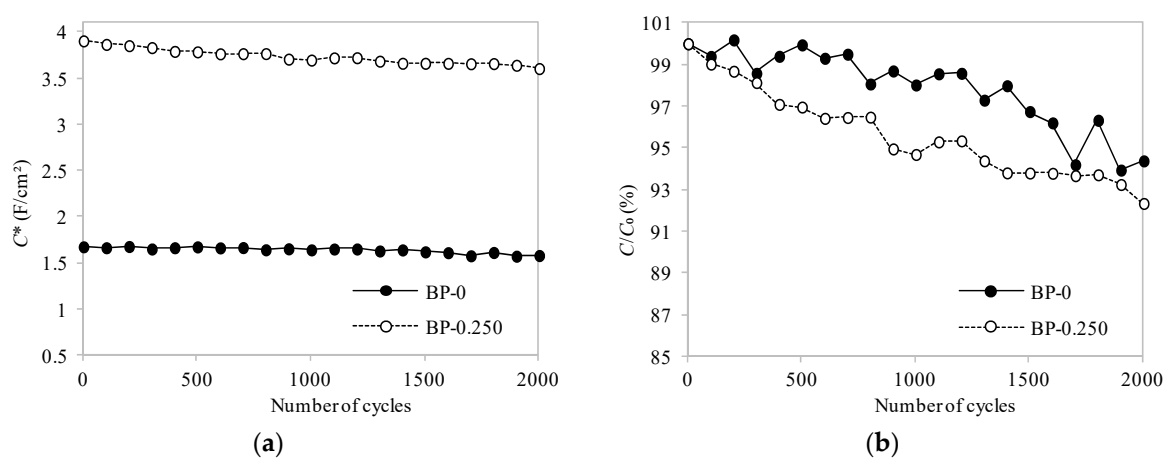


Figure 7. (a) Cyclic stability of specific capacitance C^* and (b) retention capacitance C/C_0 during long-term GCD of the composites at a current density of 10 mA/cm^2 for 2000 cycles.

The electrochemical characteristics of BP-0 and BP-0.250 composites at 3rd and 2000th galvanostatic charge–discharge cycles are shown in Table 1. Figure 8 demonstrates the comparison of CV curves at a sweep rate of 10 mV/s for these composites before and after 2000 cycles.

Table 1. Changes in electrochemical characteristics of BP-0 and BP-0.250 samples at 3rd and 2000th galvanostatic charge–discharge cycles.

Sample	C^* (F/cm ²)		R_{dis} (Ohm)		η_E (%)		η_Q (%)	
	at 3rd and 2000th Cycle		at 3rd and 2000th Cycle		at 3rd and 2000th Cycle		at 3rd and 2000th Cycle	
BP-0	1.68	1.58	0.541	0.585	71.4	71.2	94.1	93.9
BP-0.250	3.91	3.61	0.302	0.382	78.0	78.1	98.0	98.1

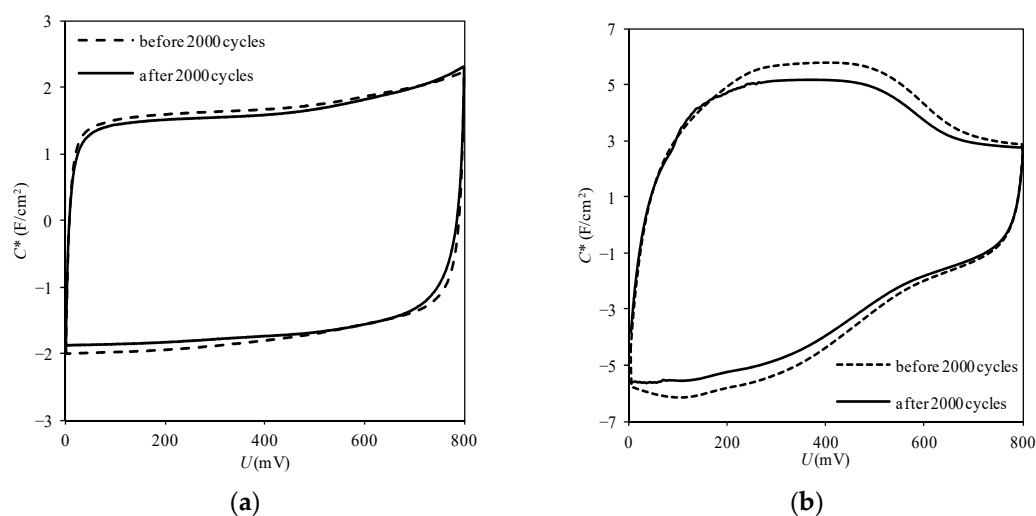


Figure 8. CV curves at 10 mV/s for (a) BP-0 and (b) BP-0.250 before and after 2000 cycles.

It is known that usually PANI as an electrode material is unstable at long-term operation; after passing 2000 charge–discharge cycles, the capacitive characteristics decrease almost twice [21,22]. The technique of using activated carbon cloth as a substrate for the formation of thin layers of PANI proposed in the present work resulted in composites with high stability of capacitive characteristics. Thus, the experiments showed that after 2000 charge–discharge cycles, the composite BP-0.250 retains about 92% of its capacitance while unmodified CC—about 94%.

Figure 9 shows diagrams demonstrating the contribution, estimated by the Trasatti method, of the specific «inner» C_i and «outer» C_o capacitances to the total specific electrical capacitance of supercapacitor cells with electrode materials based on unmodified CC BP-0 and composites BP-0.125 and BP-0.250 before 2000 cycles (Figure 9a) and for BP-0 and BP-0.250 after 2000 cycles (Figure 9b).

The diagram shows that 84% of the total specific capacitance C_T for the unmodified CC is due to the «outer» capacitance C_o , which is correlated in the Trasatti method with the capacitance of the EDL, while 16% is due to the «inner» pseudocapacitance C_i . The BP-0.125 composite showed more than double increase of the total specific capacitance, 85% of which identified as double-layer capacitance and 15% as pseudocapacitance. The BP-0.250 composite is characterized by an even larger increase in total capacitance, 73% of which is also related to double-layer capacitance and 27% to pseudocapacitance. Both capacitance components (C_i and C_o) for the composites increase in absolute values compared to the unmodified CC. At the same time, the specific surface area determined by the BET method was 1271 m²/g for unmodified CC BP-0 and 31 m²/g for the BP-0.250 composite, while the pore volume and radius determined by the BJH method were 0.51 cm³/g and 1.91 nm,

respectively, for BP-0 and $0.11 \text{ cm}^3/\text{g}$ and 1.91 nm , respectively, for BP-0.250. It should be noted that, firstly, the measured value of the specific surface for the PANI-modified CC, apparently, does not correspond to the value of the surface available to the electrolyte in the composite; during gas adsorption, the polymer is in a dried state with high density and low gas permeability, while in the electrolyte PANI swells and turns out to be permeable to a certain extent both for the solvent and for a significant part of ions. The latter makes the surface of the electrode material which is accessible for the electrolyte higher than that determined by gas adsorption. Secondly, the high proportion of EDL capacitance in PANI-modified CC electrodes is also a result of the specificity of electrochemical processes during PANI charging and discharging, which generates corresponding terminological difficulties [9]. On the one hand, these processes include changes in the electronic state of atoms (their oxidation state), i.e., they have a faradic, chemical nature, and therefore can be regarded as pseudocapacitance. On the other hand, electrically conductive polymers have metallic-type electrical conductivity, and therefore the process of charge transfer and accumulation in them proceeds in the same way as it occurs in metals, i.e., the resulting electrical capacitance is double-layer in nature. Therefore, the question of whether to consider the process as EDL charging or as Faraday pseudocapacitance depends on whether delocalized conduction band electrons are involved, or conversely, local changes in the degree of oxidation in the monomeric links of the polymer chain. It is assumed [9] that initially, at low oxidation states, the process of the second type is more pronounced, while at higher oxidation degrees, the charge centers become more and more delocalized, as a result of which the charge process changes its type to a double-layer one. Comparison of Figure 9a,b shows that in both cases of the unmodified CC and the composite, the decrease of capacitance occurs to a certain degree mainly because of pseudocapacitance lowering (0.30 to 0.25 F/cm^2 for BP-0 and 1.22 to 0.90 F/cm^2 for BP-0.250) while the double layer capacitance changes negligibly (1.52 to 1.49 F/cm^2 for BP-0 and 3.32 to 3.21 F/cm^2 for BP-0.250).

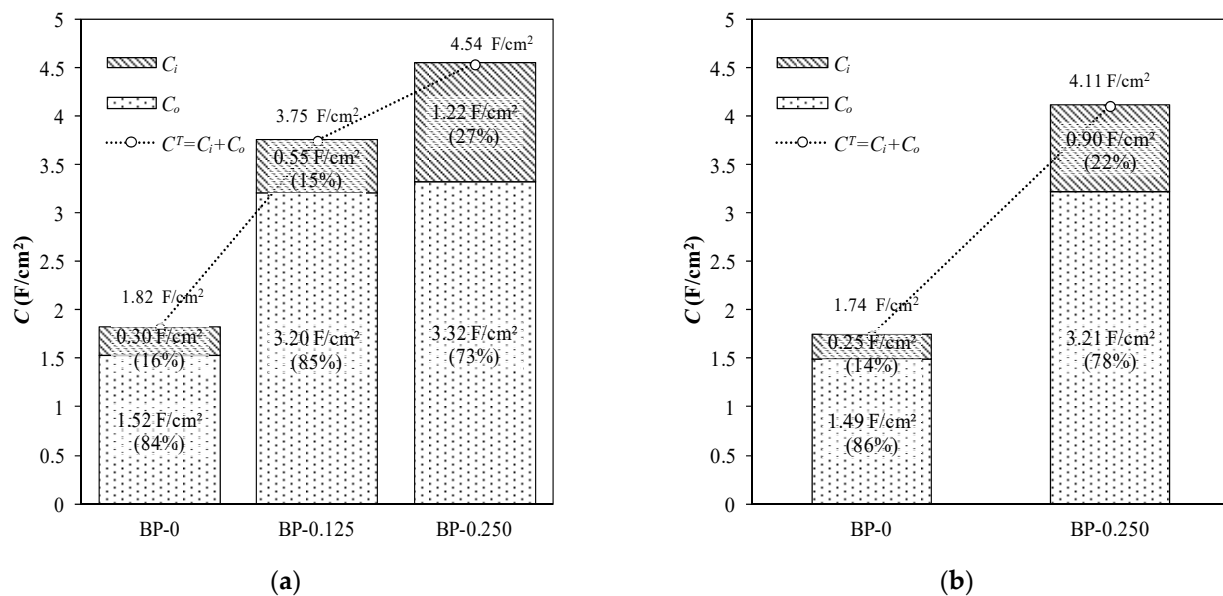


Figure 9. The results of Trasatti method CV analysis for (a) unmodified CC (BP-0) and composites BP-0.125, BP-0.250 before 2000 cycles and (b) CC BP-0 and BP-0.250 after 2000 cycles.

4. Conclusions

PANI-containing composites based on commercially available, porous, activated CC Busofit T-1-055 were obtained by chemical oxidative polymerization. It is shown that PANI is formed predominantly in the CC pores near their orifice to the carbon fiber surface. The mass fraction of the PANI in the composites is 10–12%, which is found to be sufficient to enhance the capacitive performance of the composites by more than 2.5 times compared

to unmodified CC. At the same time, a high open porosity is preserved inside the CC fibers after PANI modification, which allows energy storage to be realized also by a double-layer mechanism. Analysis of CV results for the obtained CC–PANI composites using the Trasatti method showed that the pseudocapacitance gives a much lower contribution to the total capacitance of the composite electrode material than the EDL capacitance. In the case of the composite obtained by CC modification at polymerization from a solution with 0.250 M aniline concentration, their shares are 17% and 83%, respectively, which is explained by the peculiarities of the mechanism of charge accumulation in electrically conducting polymers including the involvement of delocalized conduction band electrons in the process. The presence of a significant amount of unmodified carbon material in the CC–PANI composites causes the obtained composites to retain high values of electrical conductivity and current and energy efficiencies. Due to the fact that PANI is formed as thin layers on the developed CC surface, the composites have high lifetime stability, showing retention of more than 90% of the initial capacitance after 2000 charge and discharge cycles. The composites possess a combination of properties that make them attractive for use as SC electrode materials. The commercial availability of the materials used and the manufacturability of the composite fabrication process also contribute to the possible commercialization of the development.

Supplementary Materials: The following supporting information can be downloaded at: <https://www.mdpi.com/article/10.3390/cryst14050457/s1>: Figure S1: FTIR spectrum of BP–0.250 CC–PANI composite; Figure S2: FTIR spectrum of PANI (salt form) obtained by the oxidation of aniline by ammonium persulfate in sulfuric acid medium; Figure S3: FTIR spectrum of CC Busofit T–1–055; Figure S4a: Adsorption/desorption isotherms for BP–0 and BP–0.250; Figure S4b: Pore size distribution plots for BP–0 and BP–0.250; Figure S5: Original, uncropped, and unadjusted image of unmodified CC fibers obtained by scanning electron microscopy (Figure 1 in the main text); Figure S6a: Original, uncropped, and unadjusted image of BP–0 sample obtained by dual-beam scanning electron microscopy (Figure 2a in the main text); Figure S6b: Original, uncropped, and unadjusted image of BP–0.250 sample obtained by dual-beam scanning electron microscopy (Figure 2b in the main text); Figure S7a: Original, uncropped, and unadjusted image of BP–0 sample obtained by dual-beam scanning electron microscopy (Figure 3a in the main text); Figure S7b: Original, uncropped, and unadjusted image of BP–0 sample obtained by dual-beam scanning electron microscopy (Figure 3b in the main text); Figure S7c: Original, uncropped, and unadjusted image of BP–0.250 sample obtained by dual-beam scanning electron microscopy (Figure 3c in the main text); Figure S7d: Original, uncropped, and unadjusted image of BP–0.250 sample obtained by dual-beam scanning electron microscopy (Figure 3d in the main text).

Author Contributions: Conceptualization, S.V.S.; Methodology, S.V.S., I.S.K. and E.A.N.; Validation, K.E.S., E.S.S. and Z.E.Z.; Formal Analysis, I.S.K., K.E.S. and V.V.B.; Investigation, K.E.S., V.V.B., T.L.L. and E.S.S.; Resources, S.V.S., I.S.K. and T.L.L.; Data Curation, K.E.S., T.L.L. and V.V.B.; Writing—Original Draft Preparation, I.S.K., K.E.S. and T.L.L.; Writing—Review & Editing, S.V.S., V.V.B., E.S.S., Z.E.Z. and E.A.N.; Visualization, I.S.K., K.E.S. and E.S.S.; Supervision, S.V.S. and I.S.K.; Project Administration, T.L.L. and E.A.N.; Funding Acquisition, S.V.S. and A.M.K. All authors have read and agreed to the published version of the manuscript.

Funding: This work was supported by the Federal Academic Leadership program «Priority 2030» under the «Increase Competitiveness» program of the National University of Science and Technology MISIS, grant number K1-2022-032.

Data Availability Statement: The original contributions presented in the study are included in the article, further inquiries can be directed to the corresponding authors.

Conflicts of Interest: The authors declare no conflicts of interest.

References

1. Sun, J.; Luo, B.; Li, H. A review on the conventional capacitors, supercapacitors, and emerging hybrid Ion capacitors: Past, present, and future. *Adv. Energy Sustain. Res.* **2022**, *3*, 2100191. [[CrossRef](#)]
2. Kim, B.K.; Sy, S.; Yu, A.; Zhang, J. Electrochemical supercapacitors for energy storage and conversion. *Handb. Clean Energy Syst.* **2015**, *5*, 1–25. [[CrossRef](#)]

3. Zhao, J.; Burke, A.F. Review on supercapacitors: Technologies and performance evaluation. *J. Energy Chem.* **2021**, *59*, 276–291. [[CrossRef](#)]
4. Simon, P.; Gogotsi, Y. Materials for electrochemical capacitors. *Nat. Mater.* **2008**, *7*, 845–854. [[CrossRef](#)] [[PubMed](#)]
5. Zhang, K.; Yang, X.; Li, D. Engineering graphene for high-performance supercapacitors: Enabling role of colloidal chemistry. *J. Energy Chem.* **2018**, *27*, 1–5. [[CrossRef](#)]
6. Frackowiak, E. Carbon materials for supercapacitor application. *Phys. Chem. Chem. Phys.* **2007**, *9*, 1774–1785. [[CrossRef](#)] [[PubMed](#)]
7. Wang, Y.; Zhang, L.; Hou, H.; Xu, W.; Duan, G.; He, S.; Jiang, S. Recent progress in carbon-based materials for supercapacitor electrodes: A review. *J. Mater. Sci.* **2021**, *56*, 173–200. [[CrossRef](#)]
8. Wang, S.; Wang, X.; Sun, C.; Wu, Z.S. Room-temperature fast assembly of 3D macroscopically porous graphene frameworks for binder-free compact supercapacitors with high gravimetric and volumetric capacitances. *J. Energy Chem.* **2021**, *61*, 23–28. [[CrossRef](#)]
9. Conway, B. *Electrochemical Supercapacitors: Scientific Fundamentals and Technological Applications*, 1st ed.; Springer: New York, NY, USA, 1999; p. 698.
10. Chen, J.; Lee, P.S. Electrochemical supercapacitors: From mechanism understanding to multifunctional applications. *Adv. Energy Mater.* **2021**, *11*, 2003311. [[CrossRef](#)]
11. Şahin, M.E.; Blaabjerg, F.; Sangwongwanich, A. A comprehensive review on supercapacitor applications and developments. *Energies* **2022**, *15*, 674. [[CrossRef](#)]
12. Liu, S.; Wei, L.; Wang, H. Review on reliability of supercapacitors in energy storage applications. *Appl. Energy* **2020**, *278*, 115436. [[CrossRef](#)]
13. Olabi, A.G.; Abbas, Q.; Al Makky, A.; Abdelkareem, M.A. Supercapacitors as next generation energy storage devices: Properties and applications. *Energy* **2022**, *248*, 123617. [[CrossRef](#)]
14. Park, H.W.; Roh, K.C. Recent advances in and perspectives on pseudocapacitive materials for supercapacitors—a review. *J. Power Sources* **2023**, *557*, 232558. [[CrossRef](#)]
15. Liu, T.; Li, Y. Addressing the Achilles’ heel of pseudocapacitive materials: Long-term stability. *InfoMat* **2020**, *2*, 807–842. [[CrossRef](#)]
16. Simon, P.; Gogotsi, Y.; Dunn, B. Where do batteries end and supercapacitors begin? *Science* **2014**, *343*, 1210–1211. [[CrossRef](#)]
17. Choi, C.; Ashby, D.S.; Butts, D.M.; DeBlock, R.H.; Wei, Q.; Lau, J.; Dunn, B. Achieving high energy density and high power density with pseudocapacitive materials. *Nat. Rev. Mater.* **2020**, *5*, 5–19. [[CrossRef](#)]
18. Augustyn, V.; Simon, P.; Dunn, B. Pseudocapacitive oxide materials for high-rate electrochemical energy storage. *Energy Environ. Sci.* **2014**, *7*, 1597–1614. [[CrossRef](#)]
19. Shaikh, N.S.; Ubale, S.B.; Mane, V.J.; Shaikh, J.S.; Lokhande, V.C.; Prasertthdam, S.; Kanjanaboos, P. Novel electrodes for supercapacitor: Conducting polymers, metal oxides, chalcogenides, carbides, nitrides, MXenes, and their composites with graphene. *J. Alloys Compd.* **2022**, *893*, 161998. [[CrossRef](#)]
20. Liu, R.; Zhou, A.; Zhang, X.; Mu, J.; Che, H.; Wang, Y.; Kou, Z. Fundamentals, advances and challenges of transition metal compounds-based supercapacitors. *Chem. Eng. J.* **2021**, *412*, 128611. [[CrossRef](#)]
21. Zhao, Z.; Xia, K.; Hou, Y.; Zhang, Q.; Ye, Z.; Lu, J. Designing flexible, smart and self-sustainable supercapacitors for portable/wearable electronics: From conductive polymers. *Chem. Soc. Rev.* **2021**, *50*, 12702–12743. [[CrossRef](#)]
22. Shown, I.; Ganguly, A.; Chen, L.C.; Chen, K.H. Conducting polymer-based flexible supercapacitor. *Energy Sci. Eng.* **2015**, *3*, 2–26. [[CrossRef](#)]
23. Meng, Q.; Cai, K.; Chen, Y.; Chen, L. Research progress on conducting polymer based supercapacitor electrode materials. *Nano Energy* **2017**, *36*, 268–285. [[CrossRef](#)]
24. Sardana, S.; Gupta, A.; Singh, K.; Maan, A.S.; Ohlan, A. Conducting polymer hydrogel based electrode materials for supercapacitor applications. *J. Energy Storage* **2022**, *45*, 103510. [[CrossRef](#)]
25. Suriyakumar, S.; Bhardwaj, P.; Grace, A.N.; Stephan, A.M. Role of polymers in enhancing the performance of electrochemical supercapacitors: A review. *Batter. Supercaps* **2021**, *4*, 571–584. [[CrossRef](#)]
26. Eftekhari, A.; Li, L.; Yang, Y. Polyaniline supercapacitors. *J. Power Sources* **2017**, *347*, 86–107. [[CrossRef](#)]
27. Banerjee, J.; Dutta, K.; Kader, M.A.; Nayak, S.K. An overview on the recent developments in polyaniline-based supercapacitors. *Polym. Adv. Technol.* **2019**, *30*, 1902–1921. [[CrossRef](#)]
28. Mi, H.; Zhang, X.; Yang, S.; Ye, X.; Luo, J. Polyaniline nanofibers as the electrode material for supercapacitors. *Mater. Chem. Phys.* **2008**, *112*, 127–131. [[CrossRef](#)]
29. Agobi, A.U.; Louis, H.; Magu, T.O.; Dass, P.M. A review on conducting polymers-based composites for energy storage application. *J. Chem. Rev.* **2019**, *1*, 19–34.
30. Li, K.; Liu, X.; Chen, S.; Pan, W.; Zhang, J. A flexible solid-state supercapacitor based on graphene/polyaniline paper electrodes. *J. Energy Chem.* **2019**, *32*, 166–173. [[CrossRef](#)]
31. Liu, P.; Yan, J.; Guang, Z.; Huang, Y.; Li, X.; Huang, W. Recent advancements of polyaniline-based nanocomposites for supercapacitors. *J. Power Sources* **2019**, *424*, 108–130. [[CrossRef](#)]
32. Wang, X.; Wu, D.; Song, X.; Du, W.; Zhao, X.; Zhang, D. Review on carbon/polyaniline hybrids: Design and synthesis for supercapacitor. *Molecules* **2019**, *24*, 2263. [[CrossRef](#)]
33. Thanasamy, D.; Jesuraj, D.; Avadhanam, V.; Chinnadurai, K.; Kannan, S.K.K. Microstructural effect of various polyaniline-carbon nanotube core-shell nanocomposites on electrochemical supercapacitor electrode performance. *J. Energy Storage* **2022**, *53*, 105087. [[CrossRef](#)]

34. Panasenko, I.V.; Bulavskiy, M.O.; Iurchenkova, A.A.; Aguilar-Martinez, Y.; Fedorov, F.S.; Fedorovskaya, E.O.; Nasibulin, A.G. Flexible supercapacitors based on free-standing polyaniline/single-walled carbon nanotube films. *J. Power Sources* **2022**, *541*, 231691. [[CrossRef](#)]
35. Wang, Y.; Ding, Y.; Guo, X.; Yu, G. Conductive polymers for stretchable supercapacitors. *Nano Res.* **2019**, *12*, 1978–1987. [[CrossRef](#)]
36. Ren, L.; Zhang, G.; Lei, J.; Wang, Y.; Hu, D. Novel layered polyaniline-poly (hydroquinone)/graphene film as supercapacitor electrode with enhanced rate performance and cycling stability. *J. Colloid Interface Sci.* **2018**, *512*, 300–307. [[CrossRef](#)]
37. Vonlanthen, D.; Lazarev, P.; See, K.A.; Wudl, F.; Heeger, A.J. A stable polyaniline-benzoquinone-hydroquinone supercapacitor. *Adv. Mater.* **2014**, *26*, 5095–5100. [[CrossRef](#)]
38. Wang, G.; Wang, H.; Lu, X.; Ling, Y.; Yu, M.; Zhai, T.; Li, Y. Solid-state supercapacitor based on activated carbon cloths exhibits excellent rate capability. *Adv. Mater.* **2014**, *26*, 2676–2682. [[CrossRef](#)]
39. Liu, X.; Xu, W.; Zheng, D.; Li, Z.; Zeng, Y.; Lu, X. Carbon cloth as an advanced electrode material for supercapacitors: Progress and challenges. *J. Mater. Chem. A* **2020**, *8*, 17938–17950. [[CrossRef](#)]
40. Mishra, A.; Shetti, N.P.; Basu, S.; Raghava Reddy, K.; Aminabhavi, T.M. Carbon cloth-based hybrid materials as flexible electrochemical supercapacitors. *ChemElectroChem* **2019**, *6*, 5771–5786. [[CrossRef](#)]
41. Han, X.; Huang, Z.H.; Meng, F.; Jia, B.; Ma, T. Redox-etching induced porous carbon cloth with pseudocapacitive oxygenic groups for flexible symmetric supercapacitor. *J. Energy Chem.* **2022**, *64*, 136–143. [[CrossRef](#)]
42. Ouyang, Y.; Huang, R.; Xia, X.; Ye, H.; Jiao, X.; Wang, L.; Hao, Q. Hierarchical structure electrodes of NiO ultrathin nanosheets anchored to NiCo₂O₄ on carbon cloth with excellent cycle stability for asymmetric supercapacitors. *Chem. Eng. J.* **2019**, *355*, 416–427. [[CrossRef](#)]
43. Li, H.; Liang, J.; Li, H.; Zheng, X.; Tao, Y.; Huang, Z.H.; Yang, Q.H. Activated carbon fibers with manganese dioxide coating for flexible fiber supercapacitors with high capacitive performance. *J. Energy Chem.* **2019**, *31*, 95–100. [[CrossRef](#)]
44. Zhang, H.; Xiao, D.; Li, Q.; Ma, Y.; Yuan, S.; Xie, L.; Lu, C. Porous NiCo₂O₄ nanowires supported on carbon cloth for flexible asymmetric supercapacitor with high energy density. *J. Energy Chem.* **2018**, *27*, 195–202. [[CrossRef](#)]
45. Zhu, C.; He, Y.; Liu, Y.; Kazantseva, N.; Saha, P.; Cheng, Q. ZnO@ MOF@ PANI core-shell nanoarrays on carbon cloth for high-performance supercapacitor electrodes. *J. Energy Chem.* **2019**, *35*, 124–131. [[CrossRef](#)]
46. Horng, Y.Y.; Lu, Y.C.; Hsu, Y.K.; Chen, C.C.; Chen, L.C.; Chen, K.H. Flexible supercapacitor based on polyaniline nanowires/carbon cloth with both high gravimetric and area-normalized capacitance. *J. Power Sources* **2010**, *195*, 4418–4422. [[CrossRef](#)]
47. Cheng, Q.; Tang, J.; Ma, J.; Zhang, H.; Shinya, N.; Qin, L.C. Polyaniline-coated electro-etched carbon fiber cloth electrodes for supercapacitors. *J. Phys. Chem. C* **2011**, *115*, 23584–23590. [[CrossRef](#)]
48. Bian, L.J.; Luan, F.; Liu, S.S.; Liu, X.X. Self-doped polyaniline on functionalized carbon cloth as electroactive materials for supercapacitor. *Electrochim. Acta* **2012**, *64*, 17–22. [[CrossRef](#)]
49. Hong, X.; Fu, J.; Liu, Y.; Li, S.; Liang, B. Strawberry-like carbonized cotton Cloth@ Polyaniline nanocomposite for high-performance symmetric supercapacitors. *Mater. Chem. Phys.* **2021**, *258*, 123999. [[CrossRef](#)]
50. Wang, Y.; Zhu, Z.; Chen, J.; Chu, L.; Sun, F.; Li, W.; Wang, W. Homogeneously deposited polyaniline on etched porous carbon cloth towards advanced supercapacitor electrode. *Ionics* **2023**, *29*, 4887–4895. [[CrossRef](#)]
51. Graves, D.A.; Theodoroviez, L.B.; de Oliveira, T.C.; Cividanes, L.S.; Ferreira, N.G.; Almeida, D.A.; Gonçalves, E.S. Enhanced electrochemical properties of polyaniline (PANI) films electrodeposited on carbon fiber felt (CFF): Influence of monomer/acid ratio and deposition time parameters in energy storage applications. *Electrochim. Acta* **2023**, *454*, 142388. [[CrossRef](#)]
52. Gao, S.; Mi, H.; Li, Z.; Ji, C.; Sun, L.; Yu, C.; Qiu, J. Porous polyaniline arrays oriented on functionalized carbon cloth as binder-free electrode for flexible supercapacitors. *J. Electroanal. Chem.* **2019**, *848*, 113348. [[CrossRef](#)]
53. Ahirrao, D.J.; Pal, A.K.; Singh, V.; Jha, N. Nanostructured porous polyaniline (PANI) coated carbon cloth (CC) as electrodes for flexible supercapacitor device. *J. Mater. Sci. Technol.* **2021**, *88*, 168–182. [[CrossRef](#)]
54. Quijada, C.; Leite-Rosa, L.; Berenguer, R.; Bou-Belda, E. Enhanced adsorptive properties and pseudocapacitance of flexible polyaniline-activated carbon cloth composites synthesized electrochemically in a filter-press cell. *Materials* **2019**, *12*, 2516. [[CrossRef](#)] [[PubMed](#)]
55. Stejskal, J.; Sapurina, I. Polyaniline: Thin films and colloidal dispersions (IUPAC Technical Report). *Pure Appl. Chem.* **2005**, *77*, 815–826. [[CrossRef](#)]
56. Isacfranklin, M.; Yuvakkumar, R.; Ravi, G.; Velauthapillai, D.; Pannipara, M.; Al-Sehemi, A.G. Superior supercapacitive performance of Cu₂MnSnS₄ asymmetric devices. *Nanoscale Adv.* **2021**, *3*, 486–498. [[CrossRef](#)]
57. Trchová, M.; Stejskal, J. Polyaniline: The infrared spectroscopy of conducting polymer nanotubes (IUPAC Technical Report). *Pure Appl. Chem.* **2011**, *83*, 1803–1817. [[CrossRef](#)]
58. Harada, I.; Furukawa, Y.; Uedam, F. Vibrational spectra and structure of polyaniline and related compounds. *Synth. Met.* **1989**, *29*, 303–312. [[CrossRef](#)]

Disclaimer/Publisher’s Note: The statements, opinions and data contained in all publications are solely those of the individual author(s) and contributor(s) and not of MDPI and/or the editor(s). MDPI and/or the editor(s) disclaim responsibility for any injury to people or property resulting from any ideas, methods, instructions or products referred to in the content.